Journal of the European Ceramic Society **19** (1999) 2217–2231

PII: S0955-2219(99)00094-1
0955-2219/99/$ - see front matter

Microstructural Stability at Elevated Temperatures

Alan J. Ardell

Department of Materials Science and Engineering, University of California, Los Angeles, CA 90095-1595, USA

Abstract

The factors affecting the diffusion-controlled coarsening of microstructures at elevated temperatures are reviewed in this paper. Coarsening can occur in a variety of different ways. Perhaps the most familiar of these is Ostwald ripening of a dispersed phase, e.g. precipitates in a 2-phase alloy. However, there are other related Ostwald-ripening-types of processes, including coarsening of dispersed phases in 2-dimensions (e.g. precipitates in thin films, 'fibers' in directionally solidified eutectics) and coarsening of particles that grow in three dimensions in a 2-dimensional diffusion field (e.g. grain-boundary precipitates, particles on a substrate). Coarsening by fault migration, which is an important issue in the microstructural stability of directionally solidified rod and lamellar eutectics, and discontinuous coarsening, which affects the stability of cellular microstructures produced by discontinuous precipitation, eutectoid decomposition and eutectic solidification, are also discussed. The principal predictions of theories of these various types of coarsening mechanisms are described, and exemplified where possible by reference to published data. Emphasis is placed on ability of current theory to explain existing data obtained from real as well as computer simulation experiments. Possible reasons for the shortcomings of theory are discussed. © *1999 Elsevier Science Ltd. All rights reserved.*

Keywords: coarsening, modeling, microstructure-final, diffusion.

1 Introduction

The stability of the microstructure of a multiphase material at elevated temperatures is often governed by its resistance to coarsening, irrespective of whether the material is metallic, ceramic, electronic or polymeric in nature. This statement applies principally to materials that are near equilibrium in terms of their compositions and the number of dispersed phases. Coarsening involves the growth of large microstructural constituents at the expense of small ones in a polydisperse assembly, in which the sizes of the constituents are statistically distributed. The average size of the constituents increases with time while its volume fraction, f, remains nearly constant, though f must in fact increase with time towards its equilibrium value f_e. Particle coarsening in three dimensions (Ostwald ripening 3-D) is the last of the three stages in a classical precipitation reaction, nucleation and growth being the preceding two. The driving force for coarsening is the reduction of interfacial area, hence energy, that accompanies growth as solute atoms are transferred from small to large particles. The rate of solute transfer is most frequently controlled by the diffusion of solute atoms, though interface-reaction control is possible in principle; only diffusion-controlled coarsening is considered herein.

Coarsening can occur by conventional Ostwald ripening, ripening enabled by the motion of faults in the microstructure, or by discontinuous coarsening. In the context of this paper conventional Ostwald ripening refers inclusively to the phenomena of 3-D coarsening, 2-D coarsening, coarsening of 3-D particles in a 2-D diffusion field (e.g. coarsening of grain-boundary precipitates), and the coarsening of 3-D particles in a 1-D diffusion field (e.g. coarsening of precipitates on dislocations). Ripening that occurs by the motion of faults in the microstructure competes with 2-D coarsening as a mechanism adversely affecting the stability of directionally solidified rod-eutectics, and is the only mechanism for the coarsening of lamellar eutectics. Discontinuous coarsening occurs in cellular microstructures, which consist of alternating lamellae of the two product phases. This kind of microstructure evolves during discontinuous precipitation from supersaturated solid solution, eutectoid decomposition and eutectic solidification. During discontinuous coarsening the original cells or colonies are replaced by new ones with much larger spacings, sometimes as much as 20 times bigger, which nucleate at boundaries between the old cells.

The various mechanisms of coarsening will be reviewed in this paper, except for the relatively unimportant case of coarsening of 3-D particles in a 1-D diffusion field. The principal predictions of the important theories will be presented, and wherever possible will be exemplified using data from the literature. The predictive capabilities of the theories will be highlighted, but as will become apparent there remain many experimental observations that cannot yet be fully explained theoretically. Due to the breadth of the topic it will not be possible to cover all the types of coarsening comprehensively, but the reader should nevertheless come away with a sense of what is well understood, what is not, and what remains to be done.

2 Ostwald Ripening

2.1 Coarsening in three dimensions

The first complete theories of diffusion-controlled coarsening were published in the seminal papers of Lifshitz and Slyozov[1] and Wagner[2] (the LSW theory), although the essential physics of the problem were contained in earlier papers by Todes[3] and Greenwood.[4] In the LSW theory the precipitates are assumed to be spherical and sparsely dispersed throughout the matrix, with mean separations that far exceed the average size. In fact, the LSW theory is strictly speaking valid only in the limit of zero f_e, and predicts the following results. The average radius, $\langle r\rangle$, obeys the equation

$$\langle r\rangle^3 - \langle r_o\rangle^3 = kt, \tag{1}$$

and the average solute concentration of the matrix, X, varies asymptotically with t as[1,5]

$$X - X_e \approx (\kappa t)^{-1/3}, \tag{2}$$

where $\langle r_o\rangle$ is the average radius at the onset of coarsening, X_e is the equilibrium solubility of the dispersed phase and the rate constants k and κ are related to the physical and thermodynamic parameters of the system. The distribution of particle sizes assumes the scaling form[1,2]

$$g(u) = \frac{4u^2}{9}\left(\frac{3}{3+u}\right)^{7/3}\left(\frac{-3/2}{u-3/2}\right)^{11/3}\exp\left(\frac{u}{u-3/2}\right); \quad u < 3/2 \tag{3}$$

where $u = r/r^*$ (r^* is the radius of a particle in unstable equilibrium with the matrix of composition X at time t; it is neither growing nor shrinking at t and is equal to $\langle r\rangle$ in the LSW theory). Though it is not often stated, it is implicit in the LSW theory that the microstructure also exhibits scaling behavior. This means that the age of the microstructure cannot be determined from different micrographs so long as the magnifications are adjusted in such a way that the average particle is the same size in all the images.

In addition to these predictions, f varies asymptotically with time as[6]

$$f \approx f_e - \frac{(1-f_e)\ell}{\Delta X_e k^{1/3}} t^{-1/3}, \tag{4}$$

where $\Delta X_e = X_\beta - X_e$, X_β is the equilibrium concentration of the β phase and ℓ is the so-called capillary length.[7] Finally, the number of particles per unit volume, N_v, obeys the asymptotic equation[8]

$$N_v \approx \frac{3f_e}{4\pi\beta k} t^{-1} - \frac{3(1-f_e)\ell}{4\pi\Delta X_c \beta k^{4/3}} t^{-4/3} \tag{5}$$

where $\beta = \langle r^3\rangle/\langle r\rangle^3$ ($=1{\cdot}13$ in the LSW theory). Equation (5) follows from (4) because $4\pi\langle r^3\rangle N_v/3 = 4\pi\beta\langle r\rangle^3 N_v/3 = f$. Note that eqn (5) predicts rather different behavior from the commonly assumed[1,2] kinetic equation $N_v \propto t^{-1}$ because of the existence of the second term.

It has been recognized for many years that the equations of the LSW theory must be modified for the effect of volume fraction. When f_e is finite the particles are, on average, closer to each other, the diffusion distances from small shrinking particles to large growing ones are smaller, so coarsening should therefore proceed at a faster rate. The diffusion problem, however, is surprisingly complex, and different approaches to its solution have produced different results. These have been summarized in several review articles.[8–10] So far, none of the theories has been quantitatively successful in describing a complete set of experimental results, but all predict that k increases as f_e increases. The temporal behavior of the process is unchanged, so that eqns (1), (2), (4) and (5) remain formally identical. However, k in eqn (1) becomes a function of f_e and κ in eqn (2) is replaced by $k/\langle u\rangle^3$, where $\langle u\rangle < 1$ when $f_e \neq 0$ (recall that $\langle u\rangle = 1$ in the LSW theory). The predictions of several selected theories [11–15] are shown in Fig. 1. The behavior predicted by the various theories differs because of the assumptions used to describe the diffusional interactions among the particles. A sampling of the different approaches used can be found in the review articles of Voorhees.[9,10] Other important consequences of finite f_e are that spatial correlations among the particles enter the picture, and the

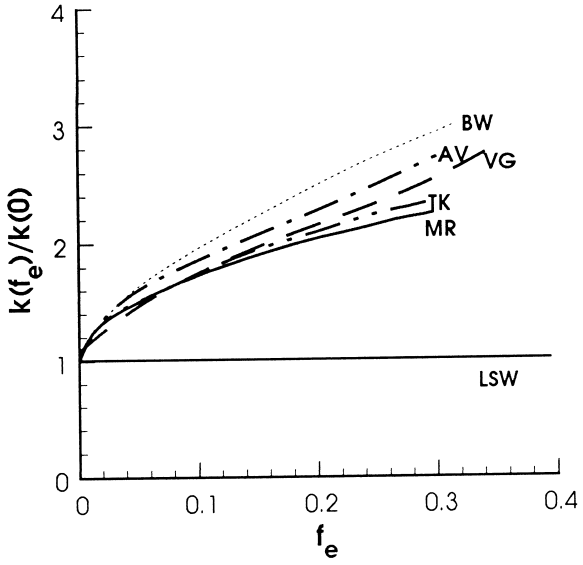

Fig. 1. Predictions of several theories of the effect of equilibrium volume fraction, f_e, on the rate constant for coarsening, $k(f_e)$, normalized by the rate constant of the LSW theory, $k(0)$. The curves shown are for the theory of Brailsford and Wynblatt (BW),[11] Marqusee and Ross (MR),[12] Tokuyama and Kawasaki (TK),[13] Voorhees and Glicksman (VG)[14] and Akaiwa and Voorhees (AV).[15].

particle size distributions become broader than the function described by eqn (3).

To illustrate the extent to which theory and experiment agree and disagree, recent data of Cho and Ardell[16,17] on the coarsening of Ni_3Si precipitates in binary Ni–Si alloys are considered here. The Ni_3Si particles have the ordered $L1_2$ (Cu_3Au) crystal structure. This alloy was chosen for investigation because the lattice mismatch, ε, between the fully coherent precipitates and the solid-solution matrix is the smallest of all binary Ni-rich Ni-base alloys containing precipitates with the identical structure type ($\varepsilon = -0{\cdot}0023$ at room temperature).[18] Also, the Ni_3Si precipitates grow to very large sizes without coalescing,[16] so that measurements are possible for long aging times; these kinds of experiments cannot be done for the more familiar Ni_3Al/Ni–Al system ($\varepsilon = 0{\cdot}0047$[18]) because elastic interactions lead to relatively early coalescence into plate-shaped precipitates when f_e exceeds about 0·1.[19] As with other binary Ni-base alloys, it is possible to measure the variation of X with t owing to the very strong dependence of the ferromagnetic Curie temperature on the solute content of the matrix solid solution phase.[20] Experiments were done for the range of volume fractions $0{\cdot}03 < f_e < 0{\cdot}30$.

The Ni_3Si particles in the alloy containing 10·98 at% Si ($f_e = 0{\cdot}0295$) are shown in Fig. 2. It is evident that the initially spherical particles acquire flat portions of their interfaces as they grow to larger sizes. The flat portions are parallel to $\langle 100 \rangle$, as they are in other Ni-base alloys. Despite the small value of ε in the Ni–Si system the particles become spatially correlated along $\langle 100 \rangle$, as they also do in other alloys; correlations are evident in Fig. 2. The data on $\langle r \rangle^3$ versus t are shown in Fig. 3

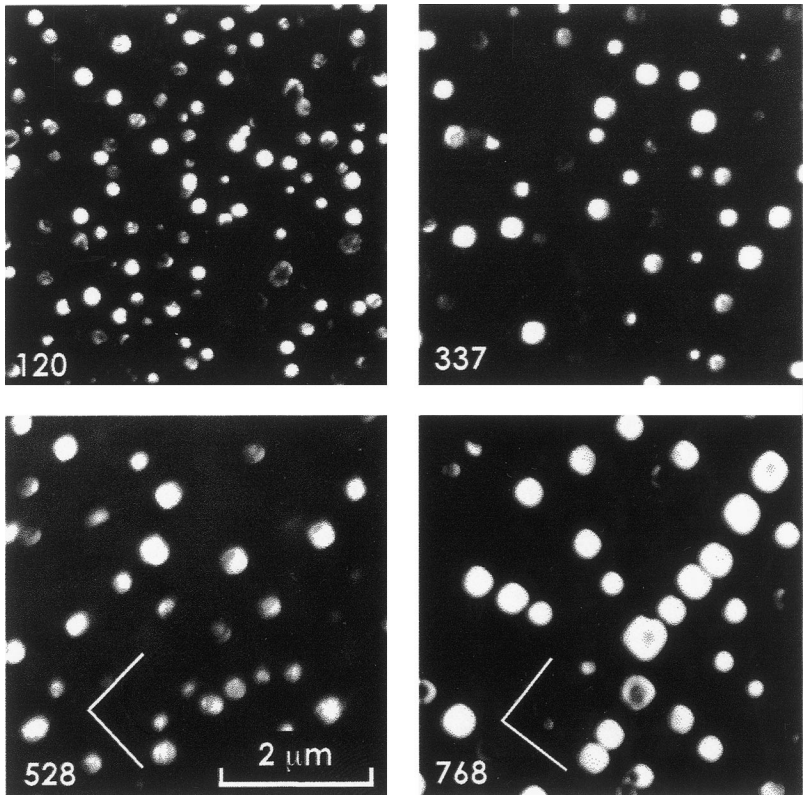

Fig. 2. Dark-field transmission electron micrographs of Ni_3Si precipitates in a Ni–10·98 at% Si alloy[17] ($f_e \approx 0{\cdot}03$) aged at 650 °C for the aging times (in h) indicated. The lines superimposed on the bottom two figures indicate the [100] and [010] directions.

and the values of k, obtained from the slopes of the curves in Fig. 3, are plotted versus f_e in Fig. 4; data from two other investigations[21,22] are included. It is evident that k does not increase as f_e increases, completely contradicting the theoretical predictions shown in Fig. 1. In fact, k appears to decrease slightly at the smallest values of f_e. This kind of behavior, also observed for the coarsening of Ni_3Al precipitates,[23] is completely at odds with theory, and has so far defied theoretical explanation. Elastic interactions among the Ni_3Si precipitates have been suggested as a possible reason. However, this is currently speculative and based in part on the significant effect of f_e on k observed for the coarsening of the δ' (Al_3Li) precipitate in binary Al–Li alloys,[24] in which $\varepsilon \approx 0$.

Particle size distributions for some of the alloys are shown in Fig. 5. It is apparent that the scaling behavior predicted theoretically is reasonably well obeyed, but the distributions are broader than the LSW distribution, and are essentially independent of f_e. The variation of X with t is shown in Fig. 6. The slopes and intercepts of the curves in Fig. 6 yield values of $\kappa^{-1/3}$ and X_e, respectively. The dependence of κ on f_e is shown in Fig. 7. The scatter is rather large, but the trend is clear; κ decreases as f_e increases, consistent with the behavior of k seen in Fig. 4. The values of X_e obtained from the intercepts in Fig. 6 are consistent with earlier measurements of the solubility limits of Si in Ni.[25]

The coarsening behavior of the Ni_3Si particles is representative of what has so far been observed in 3-D Ostwald ripening of precipitates in binary Ni-base alloys. In particular, in Ni–Al alloys k is also independent of f_e for values of f_e exceeding $\sim 0{\cdot}1$.[26] Nevertheless, the kinetic equations of the LSW theory are obeyed, and quantitative analysis of the rate constants yields values of the interfacial free energy, σ, in good agreement with theoretically calculated values, and diffusion coefficients, D, in excellent agreement with those measured in conventional diffusion experiments.[27]

The temporal behavior of N_v has not been investigated as thoroughly as those of $\langle r \rangle$ and X, but in those instances in which it has been measured the results are consistent with the predictions of eqn (4). Kirkwood[28] measured the variation with aging time of both $\langle r \rangle$ and N_v of Ni_3Al precipitates in a Ni–Al alloy. His results are shown in Fig. 8; $\langle r \rangle^3$ is plotted versus t in Fig. 8(a) and the variation of N_v with t, plotted as $N_v t$ versus $t^{-1/3}$, is shown in Fig. 8(b). If N_v were proportional to t^{-1}, as is nearly universally taken for granted, the product $N_v t$ would be constant as a function of aging time. According to eqn (4) the slopes of the curves fitted to the data in Fig. 8(b) should be negative, the magnitudes of their intercepts at $t^{-1/3} = 0$ equalling $3f_e/4\pi\beta k$. It is evident that negative

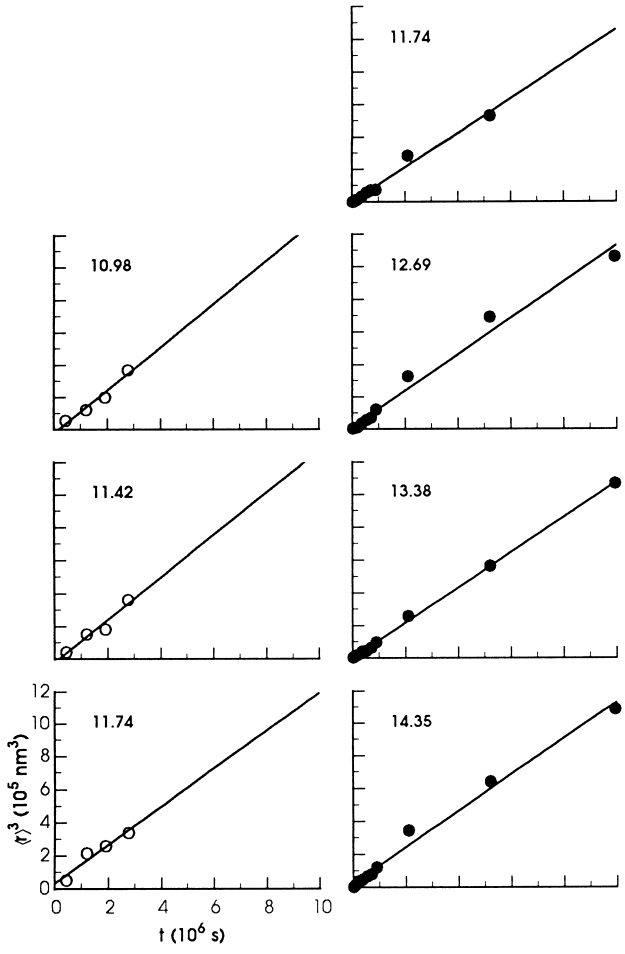

Fig. 3. Plots of the cube of the average particle sizes, $\langle r \rangle^3$, versus aging time, t, for Ni_3Si precipitates in Ni–Si alloys aged at 650 °C. The compositions of the alloys in at% Si are indicated in each figure. The open symbols refer to specimens subjected to a 'seeding' and re-aging treatment,[16] and the filled symbols refer to alloys aged conventionally.[17]

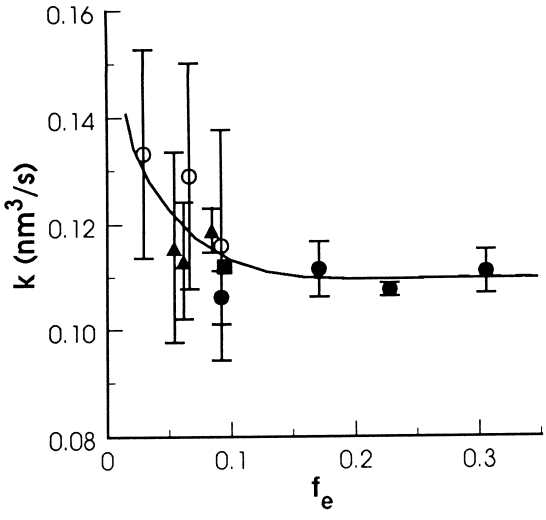

Fig. 4. The rate constants for coarsening, k, of Ni_3Si precipitates in Ni-Si alloys aged at 650 °C plotted versus the equilibrium volume fraction, f_e. The curve is drawn as a guide to the eye. The plotting symbols are: ○ Cho and Ardell,[17] seeded and re-aged; ● Cho and Ardell,[16] isothermally aged; ▲ Meshkinpour and Ardell[22] ■ Sauthoff and Kahlweit.[21]

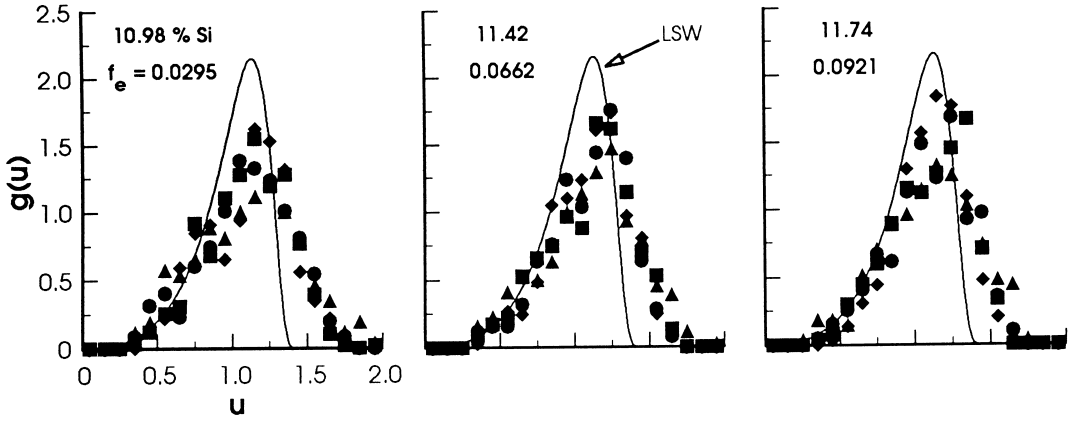

Fig. 5. Particle size distributions in three Ni–Si alloys seeded and re-aged at 650 °C[17]. The LSW distribution[1,2] is superimposed in each figure. The plotting symbols indicate aging times, in h: ■ 120; ● 337; ▲ 529; ◆ 768.

slopes are observed experimentally. The measured values of the intercepts at the two aging temperatures, and those computed using the rate constants obtained from Fig. 8(a) and the values of f_e estimated using eqn (4) as described previously,[29] with $\beta = 1{\cdot}13$, must be self-consistent if the interpretation of the data is correct. The calculated and experimentally measured intercepts are compared in Table 1. The agreement is excellent, indicating that the analysis of the data in Fig. 8 using eqn (4) passes the test of self-consistency. It has also been shown[29] that the slopes of the curves in Fig. 8 can be analyzed in a manner consistent with known values of the interfacial free energy and diffusion coefficient in the Ni_3Al/Ni–Al system.

2.2 2-D Ostwald ripening

Ostwald ripening in two dimensions can be important under certain circumstances. Two examples are ripening in thin films, in which the particles of the dispersed phase completely traverse the film thickness, and the coarsening of 'fibers' in directionally solidified rod eutectics. The theory of 2-D Ostwald ripening is formally identical to that of 3-D Ostwald ripening, but the steady-state flux of solute to a circular 'particle' is zero from an infinitely distant source (this is formally the limit of zero volume fraction). Ardell originally showed,[30] taking the effect of f_e into account using an *ad hoc* assumption relating the diffusion geometry, that the kinetics of coarsening are given by eqn (1),

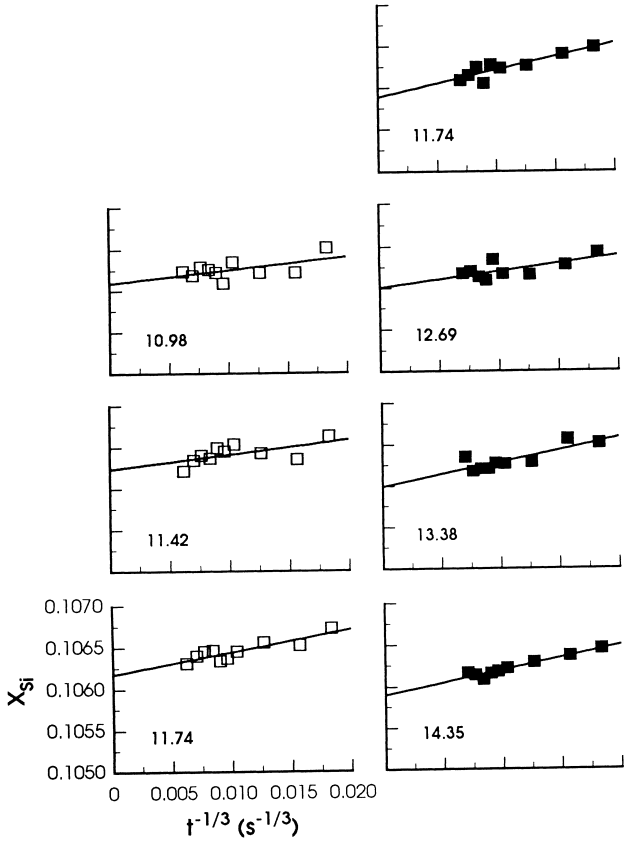

Fig. 6. The kinetics of solute depletion for the Ni–Si alloys aged at 650 °C, plotted as the variation of solute concentration in the matrix phase, X_{Si}, versus $t^{-1/3}$. The alloy concentrations are shown, and the data indicated by open symbols are from seeded and reaged specimens.[17]

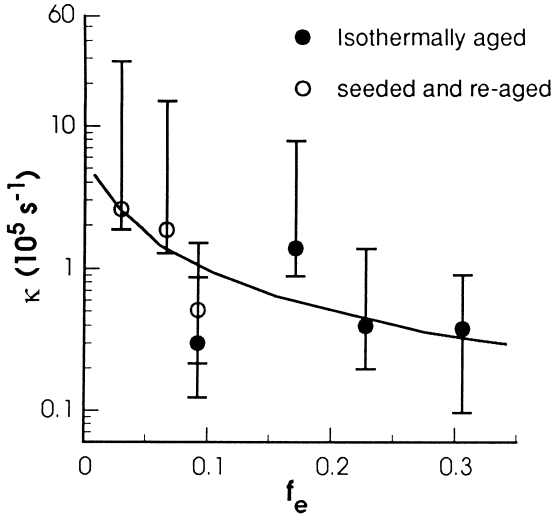

Fig. 7. The dependence of the rate constant for the kinetics of solute depletion, κ, on f_e. The open and filled plotting symbols have the same significance as in Fig. 3, and the curve is drawn as a guide to the eye. The ordinate axis is logarithmic so that the error bars can be displayed conveniently.[17]

though the dependence of k on the thermodynamic and physical parameters, as well as f_e, are different than in the case of 3-D Ostwald ripening. In the limit $f_e \rightarrow 0, k \rightarrow 0$, so that unlike the case of 3-D Ostwald ripening, coarsening in 2-D is theoretically possible *only* when f_e is finite. Nevertheless, in the limit $f_e \rightarrow 0$ the distribution of sizes remains well-behaved,[30] and is given in terms of the scaled variable $u = r/r^*$ by the equation

$$g(u) = \frac{8}{27}u^2\left(\frac{3-2u}{3}\right)^{-28/9}\left(\frac{3+u}{3}\right)^{-17/19} \times \exp\left(\frac{-4u}{3(3-2u)}\right); \quad u < 3/2. \tag{6}$$

Equation (6) was also confirmed many years later by Rogers and Desai.[31] In the limit $f_e = 0$, $\langle u \rangle = 1{\cdot}0665$,[30] so the distribution expressed in terms of the variable $r/\langle r \rangle$ differs slightly from the function described by eqn (6). The influence of f_e is to broaden the distribution, and k also increases as f_e increases. There is an implicit expectation that the microstructures should also exhibit scaling behavior.

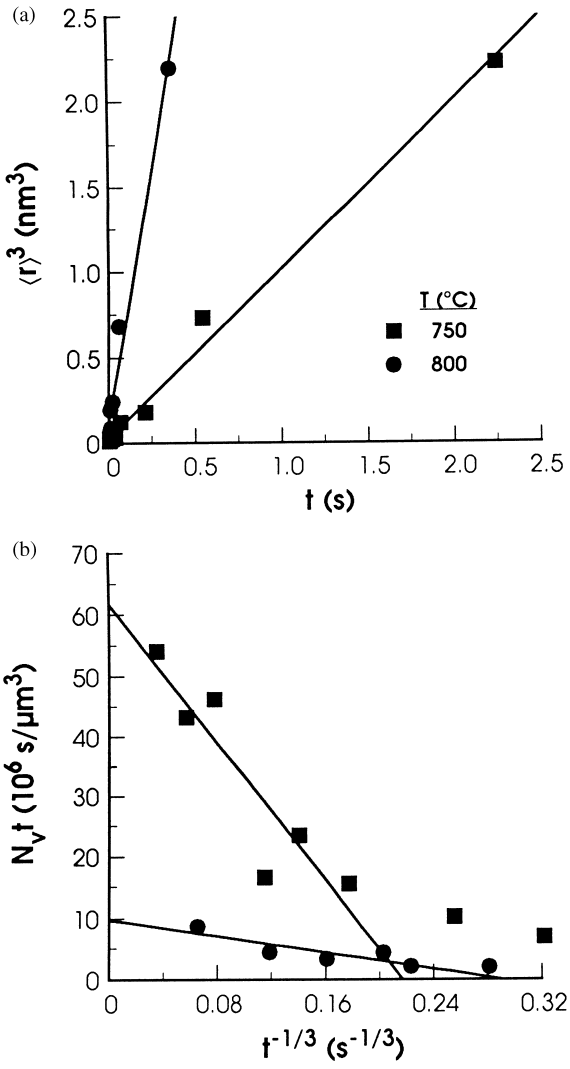

Fig. 8. The data of Kirkwood[28] on: (a) the cube of the average particle sizes, $\langle r \rangle^3$, versus aging time, t, for Ni_3Al precipitates in a Ni–13·23 at% Al alloy; (b) the variation of the number of particles per unit volume, N_v, with aging time, plotted for consistency with the predictions of eqn (5).

Table 1. Analysis of self-consistency of the data of Kirkwood[28] shown in Fig. 8 with eqns (1) and (5)

Aging temperature (°C)	f_e	k *(μm³ s⁻¹)*	*Measured intercept (s μm⁻³)*	*3 f_e/4πβk (s μm⁻³)*
750	0·0314	$9{\cdot}897\times10^{-11}$	$6{\cdot}172\times10^{7}$	$6{\cdot}706\times10^{7}$
800	0·0271	$5{\cdot}852\times10^{-11}$	$9{\cdot}743\times10^{6}$	$9{\cdot}791\times10^{6}$

The kinetics of solute depletion are formally described by eqn (2), though κ differs from its 3-D counterpart. The number of particles per unit area, N_a, in the case of 2-D Ostwald ripening decreases with t according to the equation (6):[29]

$$N_a \approx \frac{f_e}{\pi\beta k^{2/3}}t^{-2/3} - \frac{(1-f_e)\ell}{\langle u \rangle \pi\beta\Delta X_c k}t^{-1} \tag{7}$$

where $\beta = \langle r^2 \rangle / \langle r \rangle^2$ ($= 1{\cdot}038$ at $f_e = 0$). Equation (6) follows from (4) because $\pi\langle r \rangle^2 \beta N_a = f_e$.

Unlike the case with 3-D Ostwald ripening, there are only a few different theories of 2-D Ostwald ripening;[30,32–34] these nevertheless predict different dependencies of k on f_e because of different assumptions regarding the diffusion geometry. The different theories have been evaluated recently and also compared with the results of computer simulation experiments to values of f_e up to about 0·09 by Yao *et al.*[35] Their results, presented in dimensionless form, are shown in Fig. 9. It is evident that

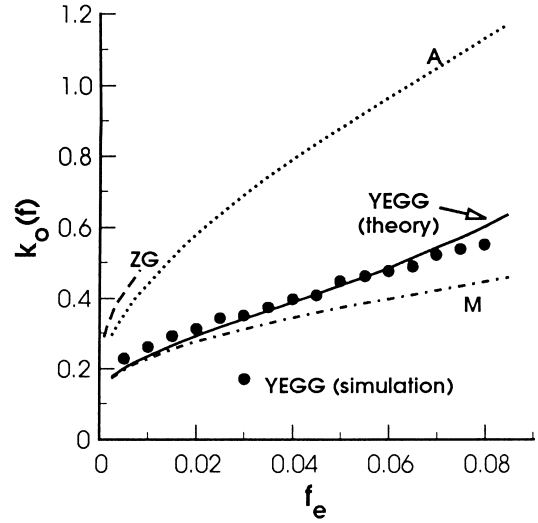

Fig. 9. The dependence of the dimensionless rate constant for 2-D Ostwald ripening, $k_o(f_e)$, on volume fraction, f_e. The results of the computer simulation experiment of Yao et al.[35] are compared with the predictions of the analytical theories of Ardell[30] (A), Marqusee[32] (M), Zheng and Gunton[33] (ZG) and Yao et al.[34] (YEGG).

the dependence of the dimensionless rate constant $k_o(=k/D\ell)$ on f_e is best described by their own theory.[34] Yao *et al.* demonstrated that their simulated particle size distributions agree best with the theory of Ardell,[30] which was also recently shown[36] to be in quite good agreement with the computer-simulated particle size distribution obtained by Rogers and Desai[31] for $f_e = 0{\cdot}3$.

Rogers and Desai[31] investigated the kinetics of decomposition in a theoretical system with a symmetrical phase diagram by numerically solving the Cahn–Hilliard equation[37] in two dimensions. Several compositions were studied, including an 'off-critical' dimensionless composition of 0·4, where the 'particles' were nearly circular throughout the entire simulation and are therefore amenable to analysis by the analytical theory. Their data are shown in Fig. 10. The plot of $\langle r\rangle^3$ versus t [Fig. 10(a)] exhibits good linearity, with a (dimensionless) slope equal to 0·374. The plot of $N_a t^{2/3}$ versus t [Fig. 10(b)] is also linear, with a negative slope as predicted by eqn (6). The parameters in eqns (1) and (6) must be self-consistent if the theory is semiquantitatively correct, hence the slope of the line in Fig. 10(a) should be consistent with the intercept $(=f_e/\pi\beta k^{2/3})$ of the line in Fig. 10(b). Taking k from Fig. 10(a) $(=0{\cdot}1222)$, with $f_e = 0{\cdot}3$,[31] the calculated value of the intercept $=0{\cdot}374$. The comparison with the experimentally determined intercept in Fig. 10(b) (0·390) is excellent, hence the set of data easily passes the test of internal consistency.

Bassereau *et al.*[38] investigated the kinetics of Ostwald ripening of 'islands' in thin films of the diblock copolymer polystyrene and polymethyl methacrylate. They measured both $\langle r\rangle$ and the variation with aging time of the actual number of particles counted in a constant area of the film, which were later converted to values of N_a. An estimate of f_e was obtained by calculating f from

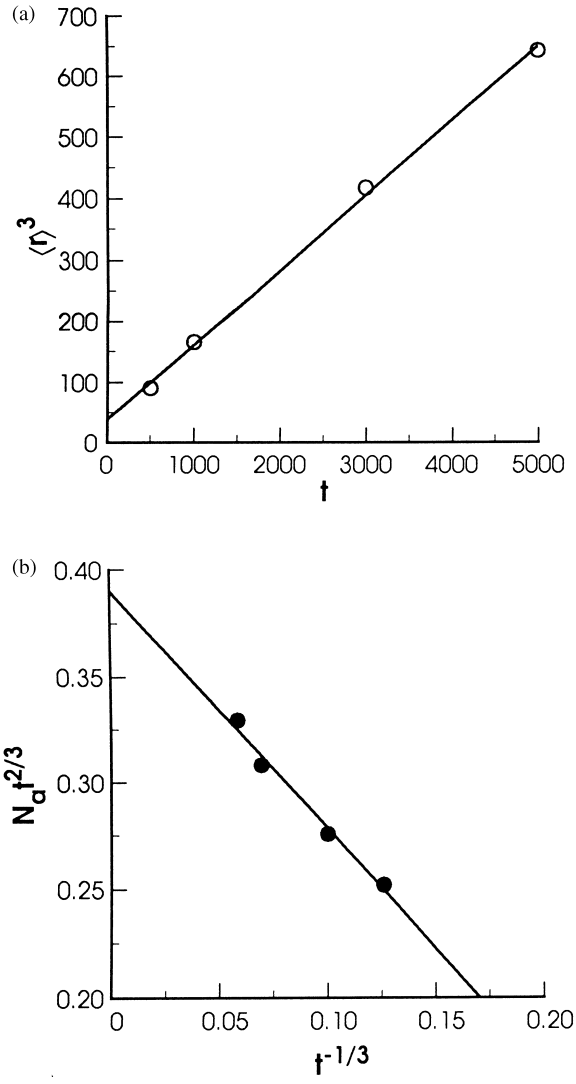

Fig. 10. The computer simulation data of Rogers and Desai[31] plotted as: (a) the cube of the average particle size, $\langle r\rangle^3$, versus aging time, t; (b) the number of particles per unit area, N_a, versus aging time plotted in a manner consistent with the predictions of eqn (6).

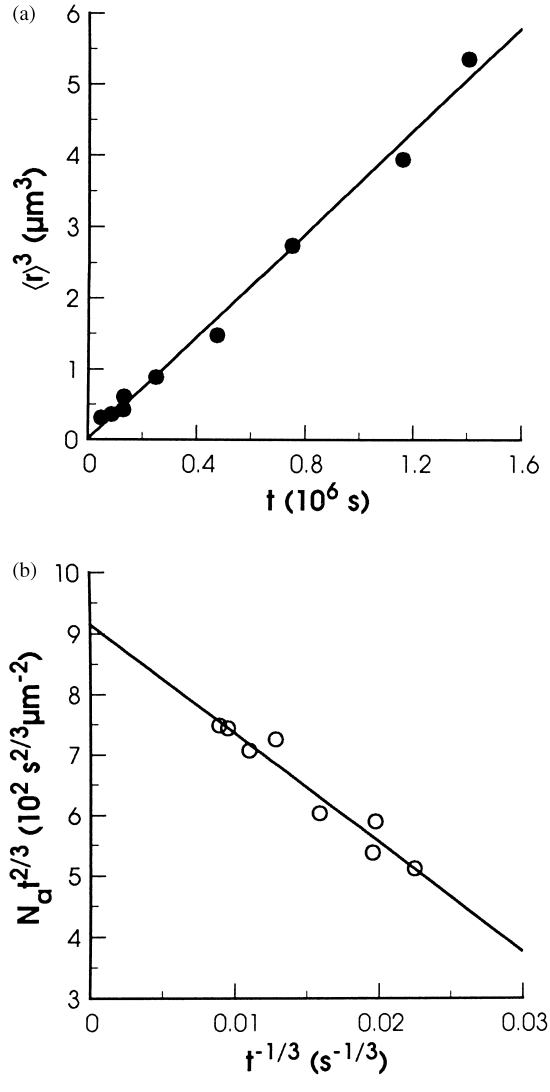

Fig. 11. Data of Bassereau et al.[38] on the coarsening of islands in a diblock copolymer film: (a) the cube of the average particle size, $\langle r\rangle^3$, versus aging time, t; (b) the number of particles per unit area, N_a, versus aging time plotted in a manner consistent with the predictions of eqn (6).

their data using the equation $\pi\beta\langle r\rangle^2 N_a = f$, plotting f versus $t^{-1/3}$ and extrapolating to $t^{-1/3} = 0$ [recall eqn (4)], yielding the result $f_e = 0{\cdot}6655$. A plot of $\langle r\rangle^3$ versus t is shown in Fig. 11(a), and a plot of $N_a t^{2/3}$ versus $t^{-1/3}$ is shown in Fig. 11(b). Using the slope of the least-squares fit to the data in Fig. 11(a), $k = 3{\cdot}618 \times 10^{-6}\,\mu m^3\,s^{-1}$, the value of the intercept in Fig. 11(b), $f_e/\beta\pi k^{2/3}$ is calculated to be $845{\cdot}8\,s^{2/3}\,\mu m^{-2}$. The measured intercept in Fig. 12(b) is $915{\cdot}5\,s^{2/3}\,\mu m^{-2}$, hence the agreement is very good and the data are internally self-consistent.

The analyses of the data on N_a of both Rogers and Desai[31] and Bassereau *et al.*[38] clearly demonstrate that the conventionally accepted kinetic law N_a versus $t^{-2/3}$ for 2-D coarsening is not obeyed for the time frames of these two investigations, otherwise the product $N_a t^{2/3}$ would be constant and independent of t for both systems.

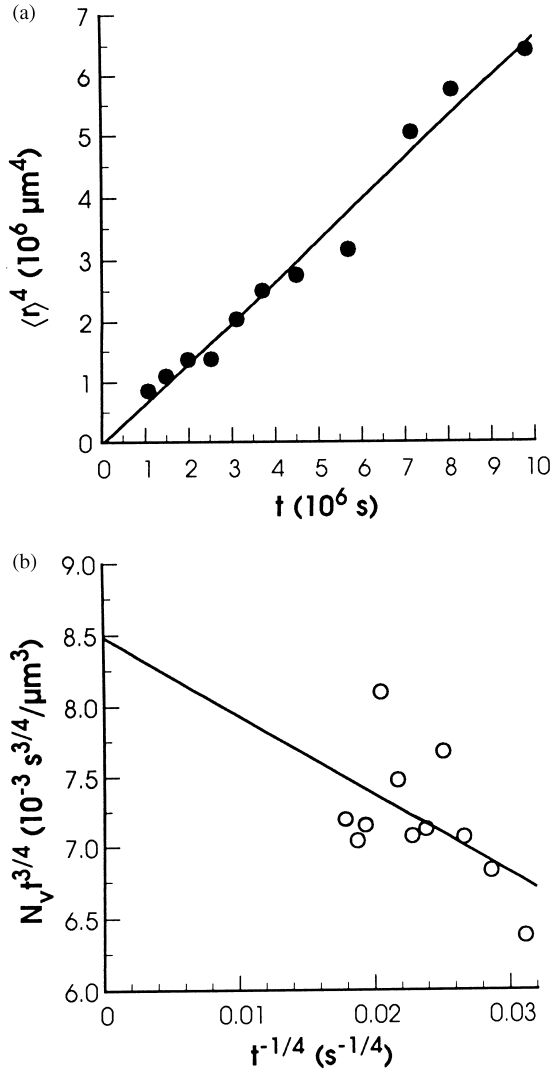

Fig. 12. The data of Rogers et al.[43] on the coarsening of SCN droplets on a quartz substrate in a solution of SCN in H_2O maintained at 42 °C: (a) the average particle size raised to the fourth power, $\langle r\rangle^4$, versus aging time, t; (b) the number of particles per unit volume, N_v, versus aging time plotted in a manner consistent with the predictions of eqn (10).

2.3 Coarsening of 3-D particles in a 2-D diffusion field

This problem was originally investigated theoretically for the case of coarsening of precipitates on grain boundaries.[39–42] The particles grow into the grains on either side of the boundary, but diffusion is limited strictly to the plane of the boundary. The temporal exponent for $\langle r\rangle$ differs from that of the previous two cases, and the kinetics of growth obey the equation

$$\langle r\rangle^4 - \langle r_o\rangle^4 = kt, \tag{8}$$

where k depends on the physical and thermodynamic parameters of the system differently than in the previous two cases considered. The kinetics of solute depletion now obey the equation

$$X - X_e \approx (\kappa t)^{-1/4}, \tag{9}$$

where κ also differs from its counterparts considered previously. Using eqn (4) and the relationship $\alpha\beta\langle r\rangle^3 N_v = f_e$, the number of particles per unit area of grain boundary, N_a, varies as

$$N_v \approx \frac{f_e}{\alpha\beta k^{3/4}} t^{-3/4} - \frac{(1-f_e)\ell}{\langle u\rangle\alpha\beta\Delta X_e k} t^{-1} \tag{10}$$

where α is a geometrical shape factor, $\beta = \langle r^3\rangle/\langle r\rangle^3 = 1{\cdot}063$ and $\langle u\rangle = 1{\cdot}0388$, the values of both parameters pertaining to $f_e = 0$. The distribution of particle sizes obeys the equation (for $f_e = 0$)[41,42]

$$g(u) = \frac{81u^3}{256}\left(1 - \frac{3u}{4}\right)^{-19/6}\left(\frac{3u^2}{16} + \frac{u}{2} + 1\right)^{-23/12} \times \exp\left\{\frac{1}{2} - \frac{2}{4-3u} - \frac{1}{6\sqrt{2}} \times \left[\tan^{-1}\left(\frac{4+3u}{4\sqrt{2}}\right) - \tan^{-1}\left(\frac{1}{\sqrt{2}}\right)\right]\right\}; \quad u < \frac{4}{3} \tag{11}$$

Although originally intended to describe coarsening on grain boundaries, eqns (9) and (11) have never been tested for that phenomenon due to lack of data. However, the equations are applicable to other physical situations, specifically coarsening of particles on a substrate. We examine data of that kind here. Rogers *et al.*[43] investigated the coarsening of droplets of succinonitrile (SCN) in water using a composition and temperature (42°C) deliberately chosen to produce identical mass densities of the two phases involved (an isopycnic system).

In such a system there should be neither sedimentation nor buoyancy of the dispersed SCN droplets. The droplets were spherical, the contact angle with the wall of the test cell being essentially 0° (the droplets were non-wetting). Coarsening was investigated over a period of about 4 months, and data were obtained using a holographic method to record their positions, number and average sizes, but not the size distributions.

The data of Rogers *et al.* on $\langle r\rangle^4$ versus t and $N_v t^{3/4}$ versus $t^{-1/4}$, as dictated by eqn (10), are shown in Fig. 12. It is apparent that the predicted linearity between $\langle r\rangle^4$ and t is well obeyed [Fig. 12(a)], but the scatter in the plot of $N_v t^{3/4}$ versus $t^{-1/4}$ is quite large [Fig. 12(b)]. The reason for the large scatter is the very small number of data points acquired in the experiments at long aging times [less than 30 particles at the three longest aging times (Dr. S. Mani, personal communication)]. Despite the scatter in Fig. 12(b), the data nevertheless satisfy the condition of self-consistency. The slope of the curve in Fig. 12(a) yields a value of $k = 0{\cdot}6677\,\mu m^4\,s^{-1}$. Using $f_e = 0{\cdot}0275$, as reported by Rogers *et al.*,[43] $\beta = 1{\cdot}063$[29] and $\alpha = 4\pi/3$ since the droplets were spherical, the calculated value of the intercept ($= 3f_e/4\pi\beta k^{3/4}$) in Fig. 12(b) should be equal to $8{\cdot}89\times10^{-3}\,s^{3/4}\,m^{-3}$. This compares quite favorably with the observed value of the intercept, $\sim 8{\cdot}5\times10^{-3}\,s^{3/4}\,m^{-3}$.

3 Coarsening of Eutectic Microstructures by Fault Migration

3.1 Rod eutectics

If rod eutectics are directionally solidified at rapid rates the morphology is often 'banded' when viewed in a longitudinal section. The bands are regions containing high densities of faults,[44] and the number of continuous fibers that completely thread the solidified structure is quite small compared to the number of faulted fibers. An example of a fault, which consists of a termination and a branch, in a rod eutectic is shown in Fig. 13. Cline[45] presented the first theory of coarsening of this type of microstructure, and Weatherly and Nakagawa[46] later modified it to yield the equation

$$N_a = N_{ao}(1 + n_o K t)^{-2}, \qquad (12)$$

where N_{ao} is the initial number of faults per unit area, n_o is the initial number of faults per unit volume and K is a rate constant which is proportional to DX_e/T.[45]

The variation of $\langle r\rangle$ with t was never explicitly stated by Cline or Weatherly and Nakagawa. However, the average diameter of the fibers must increase with time as the faults disappear, and if f is nearly constant and equal to f_e so that $\pi\langle r\rangle^2\beta N_a = f_e$, then $\langle r\rangle$ should increase with t according to the equation

$$\langle r\rangle = \langle r_o\rangle(1 + n_o K t). \qquad (13)$$

There is no reason to expect self-similarity of the particle size distributions, though this is implicitly assumed in the derivation of eqn (13) because β is taken as a time-independent constant.

The coarsening of fibers in the Al_3Ni–Al eutectic solidified at 22, 49 and 106 mm h^{-1} was investigated by Bayles *et al.*[47] Measurements of the distributions of fiber diameters were not reported, but it is evident from their published micrographs that microstructural self-similarity is not observed during coarsening. The data of Bayles *et al.* on the eutectic solidified at 106 mm h^{-1} are shown in Fig. 14(a) plotted as $N_a^{-1/2}$ versus t for consistency with eqn (12). Quantitative analysis is not possible because the parameter n_o is unknown, but an activation energy for the process can be obtained by plotting MX_e/T versus $1/T$, where M represents the slopes of the curves in Fig. 14(a). The resulting Arrhenius plot is shown in Fig. 14(b). The activation energy of coarsening is 123·2 kJ mol^{-1}, which is somewhat lower than that of diffusion of Ni in Al (145·8 kJ mol^{-1}),[48] but which nevertheless suggests that the interpretation of coarsening via fault migration is reasonable. The data of Bayles *et al.* on the eutectics solidified at the two slower rates are also consistent with the kinetics of coarsening by fault migration.

3.2 Lamellar eutectics

The coarsening of lamellar eutectics was first studied by Graham and Kraft,[49] who also developed a theory of coarsening of this type of microstructure by fault migration. The mechanism of coarsening

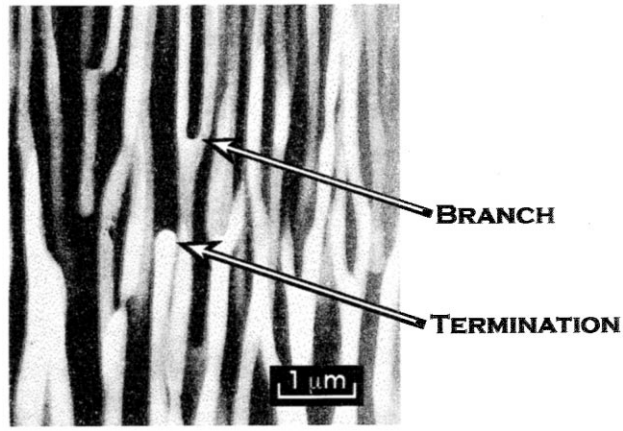

Fig. 13. Illustrating the nature of faults in a rod eutectic Al_3Ni–Al microstructure.[44] Each fault consists of a termination and a branch.

involves the diffusive transport of matter from the curved edge of a lamellar termination to a curved bulge in an adjacent lamella. The concentration gradient arises via the Gibbs–Thomson equation because the two curvatures involved are different. Using certain simplifying assumptions regarding the geometry of diffusion, and ignoring the kinetic contribution of annihilation of the faults, Graham and Kraft showed that the interphase interfacial area per unit volume, S_v, coarsens according to the kinetic law

$$S_v^{-1} - S_{vo}^{-1} = k't, \tag{14}$$

where k' is a rate constant that includes the product X_e/T. Since the lamellar spacing, λ, is related to S_v by the simple equation[50] $S_v = 2/\lambda$, eqn (14) can be rewritten in terms of λ as

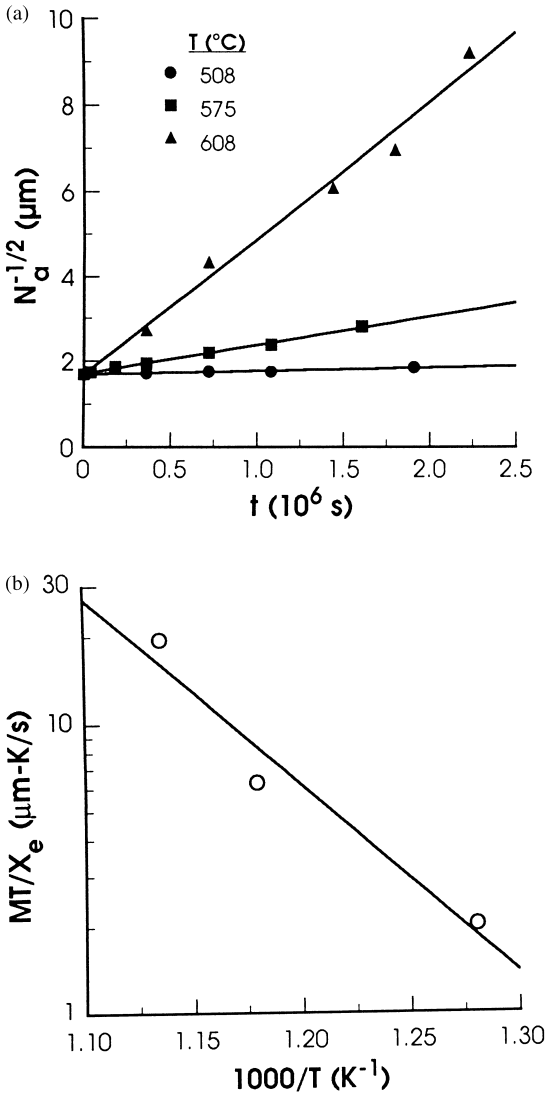

Fig. 14. The data of Bayles *et al.*[47] on the coarsening of Al_3Ni rods in the Al–Al_3Ni eutectic analyzed according to the theory of fault migration: (a) data on number of rods per unit area, N_a, plotted for consistency with eqn (12); (b) Arrhenius plot of the slopes, M, of the curves in (a) compensated for the influence of temperature, T, and equilibrium solubility, X_e.

$$\lambda - \lambda_o = 2k't, \tag{15}$$

where λ_o is the initial lamellar spacing.

Cline[45] took into account the influence of fault-annihilation on the coarsening kinetics and derived the equation

$$\lambda^2 = \lambda_o^2\left(1 + \frac{n_o k'' t}{\lambda_o}\right), \tag{16}$$

where k'' is another rate constant proportional to X_e/T. The counterpart of eqn (14) is therefore

$$S_v^{-2} = S_{vo}^{-2}\left((1 + \frac{S_{vo} n_o k'' t}{2}\right). \tag{17}$$

Neither Cline nor Graham and Kraft predicted the behavior of the distribution of lamellar spacings, but the distribution of lamellar spacings should not exhibit scaling behavior and the microstructure should not coarsen in a self-similar manner.

The stability of lamellar eutectic microstructures at elevated temperatures has been investigated only sparingly. The only study amenable to relatively straightforward interpretation is that of Graham and Kraft[49] on the Al–$CuAl_2$ eutectic. The microstructure in their alloy of eutectic composition (17·1% Cu) was lamellar when solidified at a rate of 10 mm h^{-1}. They investigated coarsening of this microstructure at three temperatures fairly close to the eutectic temperature (548 °C), and measured S_v as a function of aging time. Examples of the microstructure that evolves during coarsening are shown in Fig. 15. Coarsening is evident, but it is clearly non-uniform and the microstructure contains some lamellae that have thickened considerably and others that are nearly unchanged. There is no doubt that the lamellar microstructure is not self-similar during coarsening.

The data of Graham and Kraft are reproduced in Fig. 16, where they are plotted in the form $1/S_v$ versus t, in accordance with eqn (14). It is apparent that the coarsening kinetics at 500 and 520 °C are nearly identical, but are much faster at 540 °C. All the lines fitted to the data extrapolate to about the same point, corresponding to $S_{vo} \approx 566\,mm^{-1}$, which is consistent with the initial values reported. Using the values of k' taken from the slopes of the curves in Fig. 16(a) and the known variation of X_e with T, the activation energy obtained from an Arrhenius plot of $k'T/X_e$ versus $1/T$ [Fig. 16(b)] is 123·2 kJ mol^{-1}. The scatter in Fig. 16(b) is quite large, but the activation energy obtained agrees quite well with the published value of the activation energy for the diffusion of Cu in Al (136·1 kJ mol^{-1}).[51]

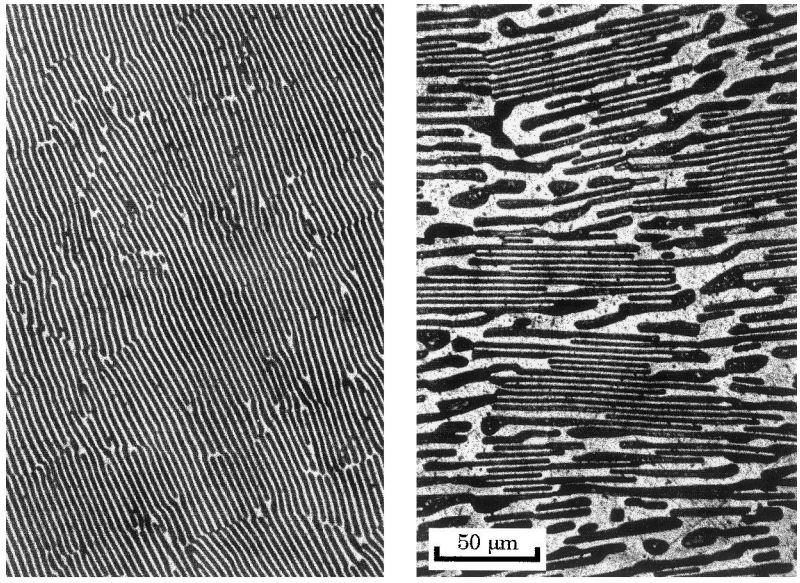

Fig. 15. Evolution of the lamellar Al–$CuAl_2$ eutectic microstructure during coarsening by fault migration,[49] observed after annealing at 1200 °C for (a) 24 h and (b) 1200 h.

The data in Fig. 16 were also analyzed according to the predictions of eqn (17), i.e. by plotting S_v^{-2} versus t and determining an activation energy from an Arrhenius plot of the temperature and concentration-compensated slopes of the curves. The activation energy so obtained, however, is 189·5 kJ mol^{-1}, which is in poorer agreement with the activation energy for the diffusion of Cu in Al than the activation energy obtained from Fig. 16(b). However, the scatter in the data of Graham and Kraft is quite large, hence it would be dangerous to conclude that eqn (7) is correct while eqn (11) is not. Clearly much more work is needed on the coarsening of lamellar eutectics before any conclusion can be drawn regarding which theory is correct.

4 Discontinuous coarsening

Discontinuous coarsening of lamellar microstructures is well known in metallurgical microstructures that evolve from discontinuous precipitation and eutectoid decomposition, and examples and references to earlier literature can be found in the paper by Livingston and Cahn,[52] who presented the first theory of this phenomenon. Instead of a continuous increase in the thickness or spacing of the lamellae with aging time, coarsening occurs by the consumption of the original lamellae by cells of new lamellae, the spacings of which, λ_2, are several times that of the original spacing, λ_1. An example of this kind of microstructure, representative of discontinuous coarsening in the Co–Si eutectoid system, is shown in Fig. 17; it is evident that the new cells nucleated at cell boundaries of the parent phases. The important microstructural features necessary for discontinuous coarsening are high-angle cell boundaries. These are ubiquitous in polycrystalline alloys that undergo discontinuous precipitation and eutectoid decomposition reactions, but have also been found in lamellar eutectic microstructures. The only example of discontinuous coarsening in a ceramic system is that of Jenecek and Pletka,[53] who investigated the phenomenon in the NiO–CaO lamellar eutectic heat-treated at 1422 °C.

The first theory of the kinetics of discontinuous coarsening was proposed by Livingston and Cahn.[52] Their theory describes the growth velocity, g, of the new cells (lamellar spacing λ_2) that consume the parent structure (lamellar spacing λ_1) as a function of the coarsening ratio $\rho = \lambda_2/\lambda_1$. Grain-boundary diffusion governs the process of atomic transport. Their equation for g is

$$g = \frac{8X_{be}}{(X_\beta - X_\alpha) f_\alpha^2 f_\beta^2} \frac{\delta D_b}{\lambda_2^2} \frac{\sigma V_m}{\lambda_1 RT} (1 - \rho^{-1}) \qquad (18)$$

where X_{be} is the equilibrium concentration in the grain boundary, X_β and X_α are the compositions of the α and β lamellae (which are not necessarily the same as their equilibrium values), f_α and f_β are the volume fractions of the α and β phases, D_b is the grain-boundary diffusivity and δ is the thickness of the grain boundary.

It is possible to test the relationship between g, ρ, λ_1 and λ_2 in eqn (18) by plotting g versus $(1 - \rho^{-1})/\lambda_1\lambda_2^2$; for a given set of data taken at constant temperature, such a plot should be linear and extrapolate to zero according to eqn (18). The data of Livingston and Cahn on discontinuous

coarsening of the NiIn-Ni2In3 eutectoid and Janecek and Pletka on discontinuous coarsening of the NiO–CaO eutectic are shown in Fig. 18. It is evident that the agreement between theory and experiment is reasonably good for the data of Livingston and Cahn, though the number of data points is limited. The same is also true for the data of Janacek and Pletka, but the intercept of the least-squares-fitted lines in Fig. 18(b) does not extrapolate to zero.

5 Discussion

There is no doubt that diffusion-controlled Ostwald ripening governs microstructural stability in the systems of the various dimensionalities considered. This can be stated with confidence despite

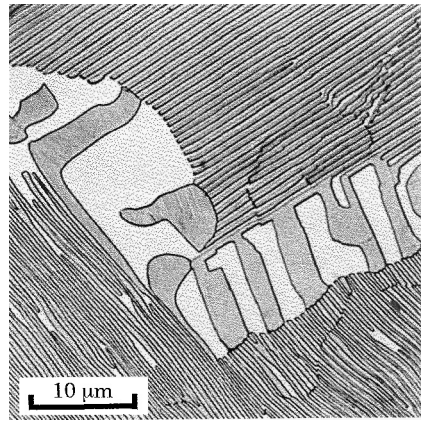

Fig. 17. Discontinuous coarsening of the lamellar Co–Co_2Si eutectoid.[52]

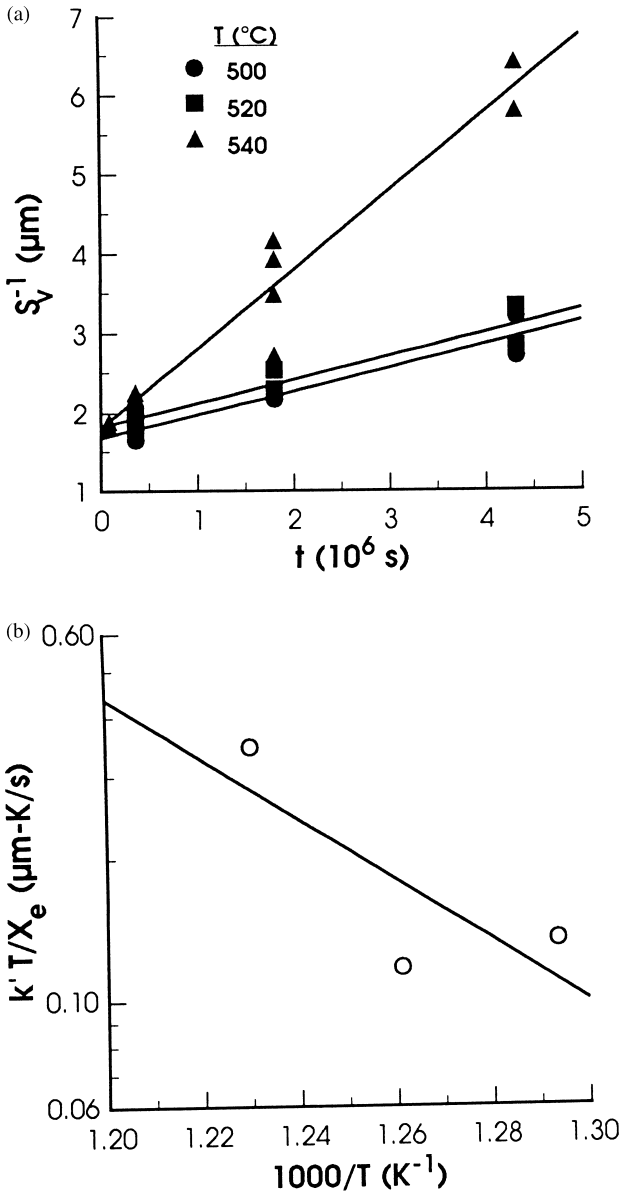

Fig. 16. The data of Graham and Kraft[49] on the coarsening of $CuAl_2$ lamellae in the Al–$CuAl_2$ eutectic analyzed according to the theory of fault migration expressed by eqn (14).

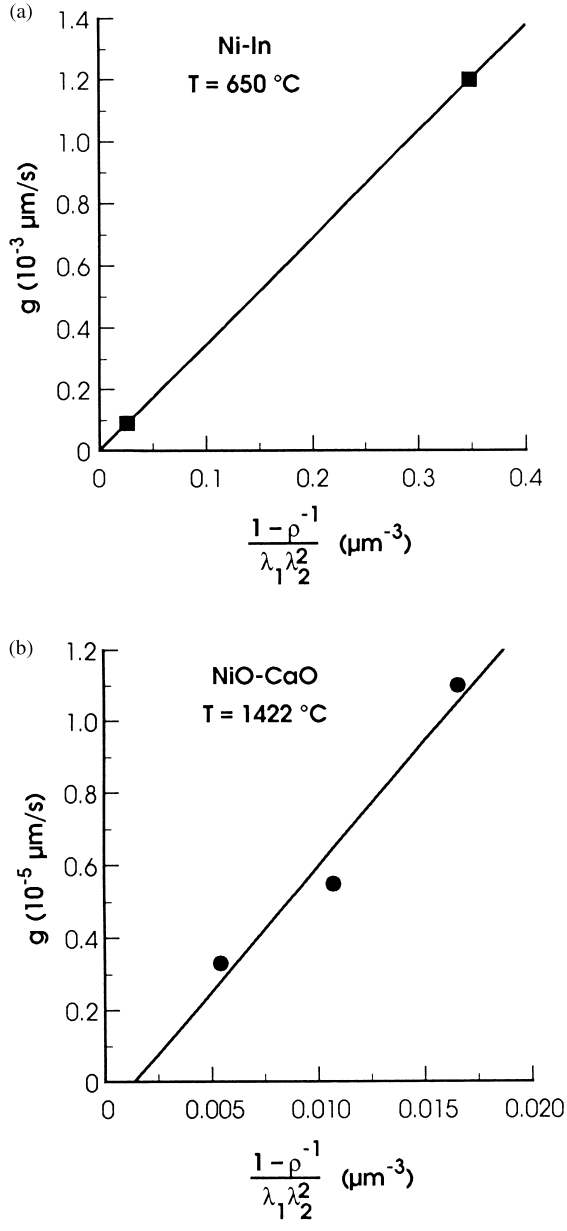

Fig. 18. Data on the growth velocity, g, plotted versus the parameter $(1-\rho^{-1})/\lambda_1\lambda_2^2$ (see text) during discontinuous coarsening: (a) the NiIn–Ni_2In_3 eutectoid,[52] $T = 650\,^{\circ}C$; (b) the NiO–CaO eutectic,[53] $T = 1422\,^{\circ}C$.

the fact that the theories are not very successful from a quantitative viewpoint. Additionally, 3-D Ostwald ripening also undoubtedly governs the kinetics of coarsening of complicated interconnected 2-phase microstructures, wherein the volume fractions of both phases are nearly equal. Spinodal decomposition can produce such microstructures, as can eutectic solidification at cooling rates that produce so-called eutectic microstructures. As has been recently shown,[54] the two microstructures can be remarkably similar, the degenerate Al–$CuAl_2$ eutectic microstructure of Graham and Kraft[49] being nearly identical in appearance to that obtained in a 2-D computer simulation experiment of Rogers and Desai,[31] which are both remarkably similar to the microstructure obtained during the spinodal decomposition of an elastically isotropic borosilicate glass.[55] There is no analytical theory of coarsening of this type of structure, but using straightforward arguments involved in analyzing the data of Graham and Kraft, relatively good agreement was obtained between the measured values of the activation energy for diffusion of Cu in Al (136·1 kJ mol^{-1}[51]) and the activation energy for coarsening of the degenerate eutectic (153·2 kJ mol^{-1}). This, plus the observation[54] that the degenerate eutectic microstructures coarsen in a self-similar manner, suggests that coarsening of degenerate eutectic microstructures is indeed consistent with the kinetics expected for 3-D Ostwald ripening.

One of the more vexing issues arising from the analyses herein is the relevancy of 2-D Ostwald ripening to the coarsening of rod eutectics. Unfortunately, there is no complete set of data on coarsening of fibers in a directionally solidified rod eutectic, i.e. no system for which the variation of $\langle r \rangle$, N_a and the fiber size distributions have all been measured. Lin *et al.*[56] and Courtney and his coworkers[57,58] concluded that coarsening of the Cr fibers in the Cu–Co eutectic and Al_3Ni fibers in the Al–Al_3Ni eutectic is governed by 2-D Ostwald ripening, especially during the earlier stages. It has been shown recently[54] that their data on N_a versus t for the Cr and Al_3Ni fibers can be analyzed according to the theories of 2-D Ostwald ripening and coarsening by fault migration equally well. Courtney[59] has argued that 2-D Ostwald ripening should dominate the early stages of coarsening if the fault density is low, but that shape instabilities can lead to pinching off of fibers, thereby producing terminations and subsequent acceleration of the kinetics. Instabilities of this type have been observed.[57,60] Perhaps the most compelling piece of evidence that 2-D Ostwald ripening controls the kinetics in the Co–Cu system is that the microstructures appear to coarsen in a self-similar manner; this is definitely not so for Al_3Ni fibers. Clearly, a thorough and comprehensive set of data on coarsening in rod eutectic systems, especially one solidified at a rate that minimizes faults in the microstructure, is needed before any conclusion can be reached about the viability of this ripening process.

There is little doubt that fault migration governs the coarsening of lamellar eutectics. Lin and Courtney[61] observed this process directly in the lamellar Pb–Sn eutectic, and the kinetic behavior predicted by the theory of Graham and Kraft[49] is in reasonably good agreement with their data. There are, however, issues in the coarsening of lamellar eutectics that have not been addressed. Not only does the microstructure of the Al–$CuAl_2$ lamellar eutectic coarsen in a non-self-similar manner (Fig. 15), but the distribution of lamellar spacings appears to be bimodal rather than unimodal. Similar characteristics can be observed in the published micrographs of Cantor and Chadwick[62] of the coarsened lamellar Al-ζ(AlAg) eutectic, in which $1/S_v$ also increases linearly with aging time. It is likely that the bimodal distribution of lamella thicknesses observed is a natural byproduct of the local nature of fault migration. It is not known whether the distribution of radii in rod eutectics evolves similarly, but it is unmistakably clear from the published micrographs of Smartt *et al.*[58] and Bayles *et al.*[47] that the distributions broaden considerably during coarsening by fault migration, and that the microstructures do not coarsen in a self-similar manner. This factor also favors coarsening of Al_3Ni rods by fault migration, because there is no reason why rod eutectic microstructures should be self-similar if they coarsen in this manner.

Information on coarsening in ceramic systems is conspicuous by its absense, except for the data of Janacek and Pletka.[53] This is not because coarsening in 2-phase ceramics is not important, but rather because there is a genuine paucity of data of the type required for the analyses described herein. Many years ago Wirtz and Fine[63] observed 3-D Ostwald ripening of precipitates of an Mg–Fe oxide in MgO. This type of behavior was subsequently confirmed by Hüther and Reppich.[64] However, neither set of data is truly complete, and the two sets do not agree. The reasons for this are not known, but the material used in the investigations was prepared by an unusual processing route, involving high-temperature diffusion anneals to make the 'alloys', followed by a lower temperature annealing treatment to promote precipitation. Other investigators have observed coarsening in other ceramic systems, including 3-D Ostwald ripening in ZrO_2 partially stabilized with MgO[65] and coarsening by a mechanism as yet to be

determined in the Al_2O_3–YAG and Al_2O_3–ZrO_2 directionally-solidified eutectics[66] (also, J.M. Yang, unpublished research). Coarsening in ceramic systems presents a rich motherlode of untapped research problems.

Despite the apparent semiquantitative agreement in Fig. 18 between the theory of Livingston and Cahn[52] and the data on discontinuous coarsening in the NiIn–Ni_2In_3 eutectoid and NiO–CaO eutectic systems, there is no theory that has quantitatively predicted g as a function of the thermodynamic and physical parameters. One outstanding issue is that there is no criterion for choosing ρ independently of g. Also, as pointed out by Fournelle,[67] eqn (18) does not take into account the excess chemical free energy that remains whenever the initial lamellae have compositions that differ from their equilibrium values. Such composition differences have been experimentally observed,[68] and the free energy associated with them must be dissipated during the approach to chemical equilibrium, thereby providing an additional driving force for discontinuous coarsening. Furthermore, recent work by Jung and Park[69] indicates that dissipation of elastic strain energy might be just as important as dissipation of interfacial and chemical free energy during discontinuous coarsening. Therefore, while discontinuous coarsening is conceptually understood, like Ostwald ripening and coarsening by fault migration, the predictive capability of existing theories is not very good.

Acknowledgements

Financial support from the National Science Foundation, the Department of Energy and the National Aeronautics and Space Administration is greatly appreciated.

References

1. Lifshitz, I. M. and Slyozov, V. V., The kinetics of precipitation from supersaturated solid solutions. *J. Phys. Chem. Solids*, 1961, **19**, 35–50.
2. Wagner, C., Theorie der alterung von niederschlägen durch umlösen (Ostwald-reifung). *Z. Electrochem.*, 1961, **65**, 581–591.
3. Todes, O. M., K teorii koagulyatzii I ukrupnenia chastitz v zolyach. II. kinetiika ukrupnenia chactitz pri 'peregonke' veshchestva cherez gomogennuyu fazy. *Zh. Fiz/Chim.*, 1946, **20**(7), 629–644.
4. Greenwood, G. W., The growth of dispersed precipitates in solutions. *Acta Metall.*, 1956, **4**, 243–248.
5. Ardell, A. J., Further applications of the theory of particle coarsening. *Acta Metall.*, 1967, **15**, 1772–1775.
6. Ardell, A. J., Experimental confirmation of the Lifshitz–Wagner theory of particle coarsening, In *The Mechanism of Phase Transformations in Crystalline Solids*. Inst. of Metals, 1969, pp. 111–116.
7. Calderon, H. A., Voorhees, P. W., Murray, J. L. and Kostorz, G., Ostwald ripening in concentrated alloys. *Acta Metall. Mater.*, 1994, **42**, 991–1000.
8. Ardell, A. J., Particle coarsening in solids: modern theories, chronic disagreement with experiment. In *Phase Transformations '87*. Inst. of Metals, 1988, pp. 485–494.
9. Voorhees, P. W., The theory of Ostwald ripening. *J. Stat. Phys.*, 1985, **38**, 231–252.
10. Voorhees, P. W., Ostwald ripening of two-phase mixtures. *Annu. Rev. Mater. Sci.*, 1992, **22**, 197–215.
11. Brailsford, A. D. and Wynblatt, P., The dependence of Ostwald ripening kinetics on particle volume fractions. *Acta Metall.*, 1979, **27**, 489–497.
12. Marqusee, J. and Ross, J., Theory of Ostwald ripening: competitive growth and its dependence on volume fraction. *J. Chem. Phys.*, 1984, **80**, 536–543.
13. Tokuyama, M. and Kawasaki, K., Statistical-mechanical theory of coarsening of spherical droplets. *Physica*, 1984, **123A**, 386–411.
14. Voorhees, P. W. and Glicksman, M. E., Solution to the multi-particle diffusion problem with applications to Ostwald ripening—II. *Computer simulations, Acta Metall.*, 1984, **32**, 2013–2030.
15. Akaiwa, N. and Voorhees, P. W., Late-stage phase separation: dynamics, spatial correlations, and structure functions. *Phys. Rev. E.*, 1994, **49**, 3860–3880.
16. Cho, J.-H. and Ardell, A. J., Coarsening of Ni_3Si precipitates in binary Ni–Si alloys at intermediate to large volume fractions. *Acta Mater.*, 1997, **45**, 1393–1400.
17. Cho, J.-H. and Ardell, A. J., Coarsening of Ni_3Si precipitates at volume fractions from 0·03 to 0·30. *Acta Mater.*, 1998, **46**, 5907–5916.
18. Kamara, A. B., Ardell, A. J. and Wagner, C. N. J., Lattice misfits in four binary Ni-base γ/γ' alloys at ambient and elevated temperatures. *Metall. Mater. Trans. A*, 1996, **27A**, 2888–2896.
19. Ardell, A. J. and Nicholson, R. B., On the modulated structure of aged Ni–Al alloys. *Acta Metall*, 1966, **14**, 1295–1309.
20. Ardell, A. J., An application of the theory of particle coarsening: the γ' precipitate in Ni–Al alloys. *Acta Metall.*, 1968, **16**, 511–516.
21. Sauthoff, G. and Kahlweit, M., Precipitation in Ni–Si alloys. *Acta Metall.*, 1969, **17**, 1501–1509.
22. Meshkinpour, M. and Ardell, A. J., Role of volume fraction in the coarsening of Ni_3Si precipitates in binary Ni–Si alloys. *Mater. Sci. Engr.*, 1994, **A185**, 153–163.
23. Maheshwari, A. and Ardell, A. J., Anomalous coarsening behavior of small volume fractions of Ni_3Al precipitates in binary Ni–Al alloys. *Acta Metall. Mater.*, 1992, **40**, 2661–2667.
24. Mahalingam, K., Gu, B. P., Liedl, G. L. and Sanders, T. H. Jr., Coarsening of δ' (Al_3Li) precipitates in binary Al–Li alloys. *Acta Metall.*, 1987, **35**, 483–498.
25. Rastogi, P. K. and Ardell, A. J., The coherent solubilities of γ' in Ni–Al, Ni–Si and Ni–Ti alloys. *Acta Metall.*, 1969, **17**, 595–602.
26. Ardell, A. J., Observations on the effect of volume fraction on the coarsening of γ' precipitates in binary Ni–Al alloys. *Scripta Metall.*, 1990, **24**, 343–346.
27. Ardell, A. J., Interfacial free energies and solute diffusivities from data on Ostwald ripening. *Interface Science*, 1995, **3**, 119–125.
28. Kirkwood, D. H., Precipitate number density in a Ni–Al alloy at early stages of ageing. *Acta Metall.*, 1970, **18**, 563–570.
29. Ardell, A. J., Temporal behavior of the number density of particles during Ostwald ripening. *Mater. Sci. Engr.*, 1997, **A238**, 108–120.
30. Ardell, A. J., Isotropic fiber coarsening in unidirectionally solidified eutectic alloys. *Metall. Trans.*, 1972, **3**, 1395–1401.
31. Rogers, T. M. and Desai, R. C., Numerical study of late-stage coarsening for off-critical quenches in the Cahn–

Hilliard equation of phase separation. *Phys. Rev. B*, 1989, **39**, 11956–11964.
32. Marqusee, J. A., Dynamics of late stage phase separations in two dimensions. *J. Chem. Phys.*, 1984, **81**, 976–981.
33. Zheng, Q. and Gunton, J. D., Theory of Ostwald ripening for two-dimensional systems. *Phys. Rev. A*, 1989, **39**, 4848–4853.
34. Yao, J. H., Elder, K. R., Guo, H. and Grant, M., Ostwald ripening in two and three dimensions. *Phys. Rev. B*, 1992, **45**, 8173–8176.
35. Yao, J. H., Elder, K. R., Guo, H. and Grant, M., Late stage droplet growth. *Physica A*, 1994, **204**, 770–788.
36. Ardell, A. J., Late-stage two-dimensional coarsening of circular clusters. *Phys. Rev. B*, 1990, **41**, 2554–2556.
37. Cahn, J. W. and Hilliard, J. E., The free energy of a non-uniform system. I. Interfacial energy. *J. Chem. Phys.*, 1958, **28**, 258–267.
38. Bassereau, P., Brodbreck, D., Russell, T. P., Brown, H. R. and Shull, K. R., Topological coarsening of symmetric diblock copolymer films: model 2D systems. *Phys. Rev. Lett.*, 1993, **71**, 1716–1719.
39. Slyozov, V. V., Coalescence of a supersaturated solid solution during diffusion along grain boundaries or dislocation lines. *Soviet Phys. Solid St.*, 1967, **9**, 927–929.
40. Speight, M. V., Growth kinetics of grain-boundary precipitates. *Acta Metall.*, 1968, **16**, 133–135.
41. Kirchner, H. O. K., Coarsening of grain-boundary precipitates. *Metall. Trans.*, 1971, **2**, 2861–2864.
42. Ardell, A. J., On the coarsening of grain boundary precipitates. *Acta Metall.*, 1972, **20**, 601–609.
43. Rogers, J. R., Downey, J. P., Witherow, W. K., Facemire, B. R., Frazier, D. O., Fradkov, V. E., Mani, S. S. and Glicksman, M. E., Coarsening of three-dimensional droplets by two-dimensional diffusion: part I. Experiment. *J. Elec. Mater.*, 1994, **23**, 999–1006.
44. Nakagawa, Y. G. and Weatherly, G. C., The thermal stability of the rod Al_3Ni–Al eutectic. *Acta Metall.*, 1972, **20**, 345–350.
45. Cline, H. E., Shape instabilities of eutectic composites at elevated temperatures. *Acta Metall.*, 1971, **19**, 481–491.
46. Weatherly, G. C. and Nakagawa, Y. G., Coarsening of rod eutectics by fault migration. *Scripta Metall.*, 1971, **5**, 777–782.
47. Bayles, B. J., Ford, J. A. and Salkind, M. J., The effect of elevated-temperature exposure on the microstructure and tensile strength of Al_3Ni whisker-reinforced aluminum. *Trans. AIME*, 1967, **239**, 844–849.
48. Erdélyi, G. D., Beke, L. and Kedves, F. J., Determination of diffusion coefficients of Zn, Co and Ni in aluminium by a resistometric method. *Phil. Mag. B*, 1978, **38**, 445–462.
49. Graham, L. D. and Kraft, R. W., Coarsening of eutectic microstructures at elevated temperatures. *Trans. AIME*, 1966, **236**, 94–102.
50. Underwood, E. E., Surface area and length in volume. In *Quantitative Microscopy*, ed. R. T. DeHoff and F. N. Rhines. McGraw–Hill, New York, 1968, pp. 77–127.
51. Bokstein, B. S., Diffusion of 3d-transition elements in aluminium. *Mater. Sci. Forum*, 1996, **217-222**, 685–688.
52. Livingston, J. D. and Cahn, J. W., Discontinuous coarsening of aligned eutectoids. *Acta Metall.*, 1974, **22**, 495–503.
53. Janecek, J. J. and Pletka, B. J., Discontinuous coarsening in directionally solidified NiO–CaO eutectics. In *Solid→Solid Phase Transformations*, ed. H. I. Aaronson, D. E. Laughlin, R. F. Sekerka and C. M. Wayman. TMS, Warrendale, 1982, pp. 963–967.
54. Ardell, A. J., Coarsening of directionally-solidified eutectic microstructures. In Proc. Int. Conf. On Computer-Aided Design of High-Temperature Materials, Santa Fe, NM, 1997.
55. Cahn, J. W. and Charles, R. J., The initial stages of phase separation in glasses. *Phys. Chem. Glasses*, 1965, **6**, 181–191.
56. Lin, L. Y., Courtney, T. H., Stark, J. P. and Ralls, K. M., The thermal stability of the fibrous copper-chromium eutectic. *Metall. Trans.*, 1976, **7A**, 1435–1441.
57. Smartt, H. B. and Courtney, T. H., The kinetics of coarsening in the Al–Al_3Ni system. *Metall. Trans.*, 1976, **7A**, 123–126.
58. Smartt, H. B., Tu, L. K. and Courtney, T. H., Elevated temperature stability of the Al–Al_3Ni eutectic composite. *Metall. Trans.*, 1971, **2**, 2717–2727.
59. Courtney, T. H., Fault migration versus two-dimensional Ostwald ripening as a mechanism for coarsening of rod eutectics. *Scripta Metall.*, 1975, **9**, 1219–1223.
60. Walter, J. L. and Cline, H. E., Stability of the directionally solidified eutectics NiAl–Cr and NiAl–Mo. *Metall. Trans.*, 1973, **4**, 33–38.
61. Lin, L. Y. and Courtney, T. H., Direct observation of lamellar fault migration in the Pb–Sn eutectic. *Metall. Trans.*, 1974, **5**, 513–514.
62. Cantor, B. and Chadwick, G. A., Thermal stability of eutectic and off-eutectic Ag-Cu, Cd-Zn and Al-ζ(AlAg) alloys. *J. Cryst. Growth*, 1976, **36**, 232–238.
63. Wirtz, G. P. and Fine, M. E., Precipitation and coarsening of magnesioferrite in dilute solutions of iron in MgO. *J. Amer. Ceram. Soc.*, 1968, **51**, 402–406.
64. Hüther, W. and Reppich, B., Order hardening of MgO by large precipitated volume fractions of spinel particles. *Mater. Sci. Engr.*, 1979, **39**, 247–259.
65. Bateman, C. A., Notis, M. R. and Williams, D. B., Coarsening kinetics of the tetragonal phase in a magnesia-partially-stabilized zirconia. *J. Amer. Ceram. Soc.*, 1972, **72**, 2372–2376.
66. Matson, L. E. and Hecht, N. Microstructural stability and mechanical properties of directionally solidified alumina/YAG eutectic monofilaments. *J. Euro. Cera. Soc.*, 1999, **19**(13–14); this issue.
67. Fournelle, R. A., Discontinuous coarsening of lamellar cellular precipitate in an austenitic Fe–30 wt%Ni–6 wt%Ti alloy-II. *Acta Metall.*, 1979, **27**, 1147–1155.
68. Yang, C. F., Sarkar, G. and Fournelle, R. A., Discontinuous precipitation and coarsening in Al–Zn alloys. *Acta Metall.*, 1988, **36**, 1511–1520.
69. Jung, J. Y. and Park, J. K., Growth kinetics of discontinuous coarsening of lamellar structure in Ti–44 at% Al (–0·5 at% Cr) intermetallic compounds. *Acta Mater.*, 1998, **46**, 4123–4130.